Opt Quant Electron
DOI 10.1007/s11082-008-9217-6

Modeling comparison of second-harmonic generation in high-index-contrast devices

Björn Maes · Peter Bienstman · Roel Baets · Bobo Hu · Phillip Sewell · Trevor Benson

Received: 11 February 2008 / Accepted: 8 May 2008

Abstract In this paper we model second-harmonic generation in a microphotonic structure using two different numerical methods. The proposed two-dimensional waveguide device is challenging as it incorporates a high-contrast grating, which instigates strong local enhancement but also radiation losses. The first simulation method extends the time-domain beam propagation method, whereas the second one builds upon frequency-domain eigenmode expansion. Good agreement between both tools is obtained for both the linear and nonlinear simulations.

Keywords Second-harmonic generation · Modeling methods · High-contrast devices

1 Introduction

Nowadays there is a strong interest in photonic integrated circuits for functions such as next-generation optical network transceivers or lab-on-a-chip sensors. In addition, by using material systems with high index contrasts the structures become more compact, have an improved performance and may be cheaper to produce. However these systems have their specific manufacturing and design challenges. For fabrication we mention e.g., the problem of sidewall roughness to obtain low-loss photonic wires. In the area of design, and more specifically numerical modeling, the appearance of high contrast instigates strong reflections and radiation losses. Great progress has been made in identifying useful methods for simulating the linear properties of these micro- and nanophotonic devices.

B. Maes (✉) · P. Bienstman · R. Baets
Department of Information Technology, Ghent University—IMEC, St.-Pietersnieuwstraat 41, 9000 Ghent, Belgium
e-mail: bjorn.maes@ugent.be

B. Hu · P. Sewell · T. Benson
George Green Institute for Electromagnetics Research, University of Nottingham, University Park, Nottingham NG7, UK

The modeling of nonlinear effects in these structures is less well studied. However, the appearance of intensity dependent effects holds the promise for many novel and useful functionalities. Second order effects e.g., can be used for versatile wavelength conversion techniques, such as second-harmonic generation (SHG), frequency up- and down-conversion, and parametric amplification. These techniques can have practical applications in laser sources, wavelength division multiplexing networks, all-optical switching, etc. Furthermore, in order to obtain effects at practical power levels it is extremely advantageous to confine the fields strongly in high index contrast waveguides and resonators.

Optical devices with second order nonlinearity have been successfully fabricated in ferroelectric materials, such as $LiNbO_3$ (Bortz and Fejer 1991), and semiconductor materials, such as $Al_xGa_{1-x}As$ (Yoo et al. 1996). In order to fully understand the function of these devices and to optimize their designs, accurate and efficient modeling techniques are needed, both for the linear and nonlinear properties.

Analytical modeling, such as the coupled-mode theory (Marcuse 1991), is quite difficult for two-dimensional (2D) or three-dimensional (3D) devices having irregular geometrical variations or radiation losses (Dumeige et al. 2003). Therefore one has to resort to numerical techniques. The Finite-Difference Time-Domain (FDTD) method is a very versatile method. It provides time-domain modeling of a pulsed beam in an arbitrary structure over a wide bandwidth (Taflove 1998). However, the method requires tremendous computational efforts, even for analyzing 2D structures (Dumeige et al. 2003).

In this paper we study two alternatives: the Time-Domain Beam-Propagation Method (TD-BPM) and the Eigenmode Expansion Method (EEM). For certain problems both methods can be orders of magnitude faster than FDTD. For TD-BPM this efficiency is rooted in the use of a carrier wave formulation and a suitable discretization scheme. For EEM efficiency stems from the frequency-domain formulation, where the field is described as a superposition of eigenmodes corresponding to piecewise-constant sections. In addition, both techniques are suited to model full-vectorial solutions in high contrast devices with strong longitudinal reflections and scattering losses. At first these methods found applications in the modeling of linear properties. However, now they have also been extended towards second-order effects.

In order to compare both methods we use a periodic grating structure, which was defined as a modeling exercise in the COST-P11 project (http://w3.uniroma1.it/energetica/). It is known that one-dimensional (1D) grating structures enhance the conversion efficacy of SHG. First of all they can bring about phase-matching, which is very important to obtain strong coherent effects. Second, the resonances of a finite device enhance the field intensities. Strong index contrasts can lower the device lengths required, as both effects are increased. However, in 2D or 3D structures the interfaces will augment scattering losses, so a trade-off becomes necessary. This argument is addressed in the design under study.

The paper is structured as follows. In the next section we describe the two modeling methods. Then we describe the proposed grating device. Subsequently, results for the linear and nonlinear case are compared and discussed.

2 Modeling methods

2.1 Time-Domain Beam Propagation Method (TD-BPM)

After being successfully implemented for the simulation of electromagnetic propagation in a general linear material (Hu et al. 2006), the Time Domain-Beam Propagation Method is now extended to analyze SHG, which has not been presented before.

Scalar wave equations for propagation of the fundamental frequency (FF) electric field E_f and the second harmonic (SH) electric field E_s are expressed as (Masoudi 2001):

$$\nabla^2 E_f = \frac{n_f^2}{c^2}\frac{\partial^2 E_f}{\partial t^2} + \mu_0 \frac{\partial^2 P_f}{\partial t^2}, \tag{1}$$

$$\nabla^2 E_s = \frac{n_s^2}{c^2}\frac{\partial^2 E_s}{\partial t^2} + \mu_0 \frac{\partial^2 P_s}{\partial t^2}, \tag{2}$$

where n_f and n_s are the refractive indices of the material considered at the fundamental and second harmonic frequencies respectively. P_f and P_s are the scalar second order nonlinear polarizations:

$$P_f = \epsilon_0 \chi_f^{(2)} E_s \cdot E_f^*, \tag{3}$$

$$P_s = \epsilon_0 \chi_f^{(2)} E_f \cdot E_f/2, \tag{4}$$

with * meaning the complex conjugate. Substituting Eqs. 3 and 4 into 1 and 2, the following is obtained:

$$\nabla^2 E_f = \frac{n_f^2}{c^2}\frac{\partial^2 E_f}{\partial t^2} + \frac{1}{c^2}\frac{\partial^2 \left(\chi_f^{(2)} E_s \cdot E_f^*\right)}{\partial t^2}, \tag{5}$$

$$\nabla^2 E_s = \frac{n_s^2}{c^2}\frac{\partial^2 E_s}{\partial t^2} + \frac{1}{c^2}\frac{\partial^2 \left(\chi_f^{(2)} E_f \cdot E_f/2\right)}{\partial t^2}. \tag{6}$$

Using the slowly varying envelope approximation (SVEA) (Benson et al. 2004), the electric fields E_f and E_s can be expressed in terms of slowly varying envelopes and fast varying carrier frequencies as:

$$E_f = \frac{1}{2}\left[\phi_f \exp(j\omega_f t) + \phi_f^* \exp(-j\omega_f t)\right], \tag{7}$$

$$E_s = \frac{1}{2}\left[\phi_s \exp(j\omega_s t) + \phi_s^* \exp(-j\omega_s t)\right], \tag{8}$$

where ϕ_f and ϕ_s are the slowly varying envelopes of the FF and SH electric fields, respectively. Inserting Eqs. 7 and 8 into 5 and 6, and neglecting the terms containing the second order derivative with respect to time according to the SVEA assumption, one obtains:

$$\begin{aligned}\nabla^2 \phi_f = {} & \frac{n_f^2}{c^2}\left(-\omega_f^2 \phi_f + 2j\omega_f \frac{\partial \phi_f}{\partial t}\right) \\ & + \frac{\chi_f^{(2)}}{c^2}\left(2\frac{\partial \phi_f^*}{\partial t}\frac{\partial \phi_s}{\partial t} + 2j\omega_f \frac{\partial \phi_f^*}{\partial t}\phi_s + 2j\omega_f \phi_f^* \frac{\partial \phi_s}{\partial t} - \omega_f^2 \phi_f^* \phi_s\right),\end{aligned} \tag{9}$$

$$\begin{aligned}\nabla^2 \phi_s = {} & \frac{n_s^2}{c^2}\left(-4\omega_f^2 \phi_s + 4j\omega_f \frac{\partial \phi_s}{\partial t}\right) \\ & + \frac{\chi_f^{(2)}}{c^2}\left(\frac{\partial \phi_f}{\partial t}\frac{\partial \phi_f}{\partial t} + 4j\omega_f \frac{\partial \phi_f}{\partial t}\phi_f - 2\omega_f^2 \phi_f \phi_f\right).\end{aligned} \tag{10}$$

The presence of the nonlinear coupling term, the last term in Eq. 9, illustrates that the FF wave is allowed to deplete during propagation with this method. Note however, for the normalized values used here, we did not include FF depletion for this exercise. The last term in Eq. 10 acts as a source to generate the SH field. Compared with the paraxial BPM

(Chou et al. 1999) and the TD-BPM technique proposed by Masoudi (2001), this formulation is bi-directional and wide-angle in nature since it does not make a paraxial approximation along the z-axis by neglecting the second order derivative of the spatial operators with respect to z. The Iterative Explicit Finite-Difference Scheme introduced in Hu (2006) can be applied to the above partial differential equations. It was demonstrated in Huang et al. (1992) that it can use a time step size at least four times bigger than the Courant-Friedrichs and Lewy stability requirement imposed on conventional time domain simulation techniques, such as the FDTD method and the transmission line modeling method. In this way the proposed algorithm can help overcome the limitations of computational intensity, a fact that makes this formulation more attractive than conventional time domain numerical techniques, especially when the 3D characterization of optical devices is examined.

For the TD-BPM simulation, the input pulse, excited at the time moment $t = 0$, consists of the fundamental mode profile ϕ_e in the transverse direction and a Gaussian profile with a $1/e$ width of 4 μm in the propagation direction. The spatial sampling mesh sizes are: $\delta x = \delta z = 0.018\,\mu\text{m}$. For the TD-BPM method, a time step size $\delta t = 4\delta z/c$ is used, again four times that required by conventional time domain simulation techniques.

Note that in this paper we compare TD-BPM to a frequency domain method. However, because TD-BPM is time domain it would also be suitable for modeling aspects related to pulse dynamics.

2.2 Eigenmode Expansion Method (EEM)

In this section we provide a succinct overview of the eigenmode method. For more information we refer to (Bienstman and Baets 2001) for modeling of linear properties, and to (Maes et al. 2005) for the SHG extension. The algorithm has been implemented in the freely available CAMFR package (Bienstman and Baets 2001).

In the EEM one defines a main propagation direction and divides the structure in piecewise constant sections, as in Fig. 1. Next, the field in such a section is described by a superposition of eigenmodes, specific to the particular section. The field profiles and propagation constants of the eigenmodes are calculated from the transversal index profile of the section or slab. In this way the electromagnetic fields in a slab are reduced to a vector of complex mode amplitudes, which describes the particular superposition of modes excited in the slab. For interfaces between different slabs one uses the established mode-matching technique to derive reflection and transmission matrices between the various modes. In the end these interface matrices are combined with the propagation properties to obtain a scattering matrix for the entire structure. If one defines a certain input excitation, this algorithm gives the mode amplitudes and thus the fields throughout the structure.

The extension for SHG proceeds as follows. We explain the algorithm in the undepleted pump approximation. First a linear simulation at the FF is performed. This gives us the FF mode amplitudes in every section of the structure. This data is used to modify the calculation of the SH. More specifically we adjust the propagation properties in a section. These are calculated as:

$$\begin{bmatrix} \mathbf{F}_2 \\ \mathbf{B}_1 \end{bmatrix} = \begin{bmatrix} \mathbf{diag}(e^{-j\beta_{SH,i}L}) & \mathbf{0} \\ \mathbf{0} & \mathbf{diag}(e^{-j\beta_{SH,i}L}) \end{bmatrix} \begin{bmatrix} \mathbf{F}_1 \\ \mathbf{B}_2 \end{bmatrix} + \begin{bmatrix} \mathbf{N}_{fw} \\ \mathbf{N}_{bw} \end{bmatrix}, \tag{11}$$

with **diag** indicating a diagonal matrix, $\beta_{SH,i}$ the propagation constant of the ith SH mode, and L the length of the section. The nonlinear change is given by the last term, $\mathbf{N}_{fw}$ and $\mathbf{N}_{bw}$. These amplitudes stem from the nonlinear polarization at the SH. They are dependent

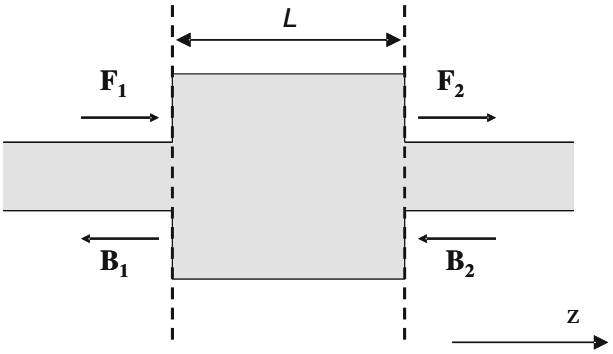

Fig. 1 Definition of a main propagation direction z and division into sections for a simple structure. Mode amplitude vectors are indicated

on the local FF amplitudes (obtained from the first calculation), overlap integrals between FF and SH modes, and phase matching factors. In the end a similar concatenation procedure for interfaces and sections as in the linear case is employed, in order to obtain the global scattering *and generation* matrices.

The advantages of this method are similar for the linear and nonlinear case. Efficiency is obtained because there is no grid necessary in the propagation direction. In addition, many structures can be calculated accurately using only a few tens of modes. The number of modes is further reduced by employing PML (perfectly-matched layer) boundary conditions, which also allows us to calculate radiation losses. Furthermore, the same sections are often reused in a device, especially in periodic structures. In these cases data such as propagation constants, overlap integrals etc. has to be calculated only once.

3 Device structure

The proposed device is a 2D model for the situation in which a 1D grating is added to a photonic waveguide. A schematic of the structure is shown in Fig. 2. The object is to exploit some of the same properties that make 1D gratings efficient for SHG. Indeed, 1D structures are shown to be good converters by using an interplay of increased density of modes at the band edge, field localization and phase matching (Centini et al. 1999; Angelis et al. 2001). The proposed 2D device combines the advantages of a waveguide structure with the benefits associated with a 1D grating structure.

As a building block of photonic devices, waveguides offer a twofold improvement: They achieve field enhancements due to their strong transverse field confinement, and they avoid

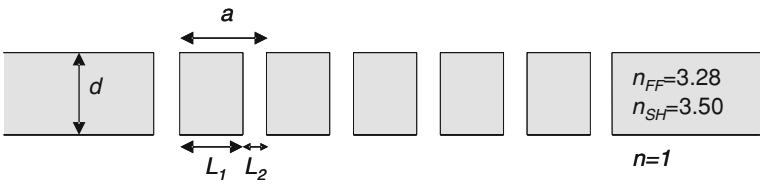

Fig. 2 Schematic of the proposed structure

the spatial walk-off between the interacting fields (Dumeige et al. 2003). Nevertheless, there are several new drawbacks associated with this structure. First, the high refractive index contrast between the layers of the grating introduces some radiation losses. Second, the single fundamental mode guiding condition should be achieved at both FF and SH frequencies. These arguments show that special care should be taken in designing such devices.

The dielectric device in Fig. 2 is surrounded by air ($n = 1$). Now, instead of modeling the full dispersive behavior of the material refractive index ($n(\omega)$), we use two separate constant values for the two frequencies, $n_{FF} = 3.28$ and $n_{SH} = 3.50$. These values correspond to the index of $Al_{0.3}Ga_{0.7}$ As around $\lambda = 1.55\,\mu m$ and $\lambda = 0.78\,\mu m$, respectively. The width of the in- and out-coupling waveguide is $d = 180\,nm$. We denote the number of periods by N. Note that N periods means $N + 1$ air slits. A period has a length of $a = 180\,nm$, divided into a dielectric part ($L_1 = 135\,nm$) and an air slit ($L_2 = 45\,nm$).

With the previous parameters the waveguide has a single TE mode for the FF around the wavelength of 1.55 µm (one electric field component, which is out-of-plane), and a single TM mode for the SH (one magnetic field component, which is out-of-plane). The device can be realized e.g. with epitaxial growth of $Al_{0.3}Ga_{0.7}$ As on a [001]-oriented GaAs substrate, by aligning the z-axis along [110]. The polarizations mentioned couple with a normalized $\chi^{(2)} = 1$, all other $\chi^{(2)}$ components are assumed to be zero.

4 Simulation results

4.1 Linear properties

To obtain the first insights about the design we model the propagation properties of an infinite structure. Thus we examine the (guided) Bloch modes of one period of the device. The EEM method, as implemented in the CAMFR package, is well suited for this. The real and the imaginary parts of the propagation constant k_z versus the frequency are shown in Fig. 3a and b, respectively. For efficient conversion, the SH is chosen so that it lies at the lower edge of the first order bandgap. In this way the interesting region for the FF is around $a/\lambda \approx 0.115$ ($\lambda \approx 1.57\,\mu m$), and for the SH around $a/\lambda \approx 0.230$ ($\lambda \approx 0.78\,\mu m$).

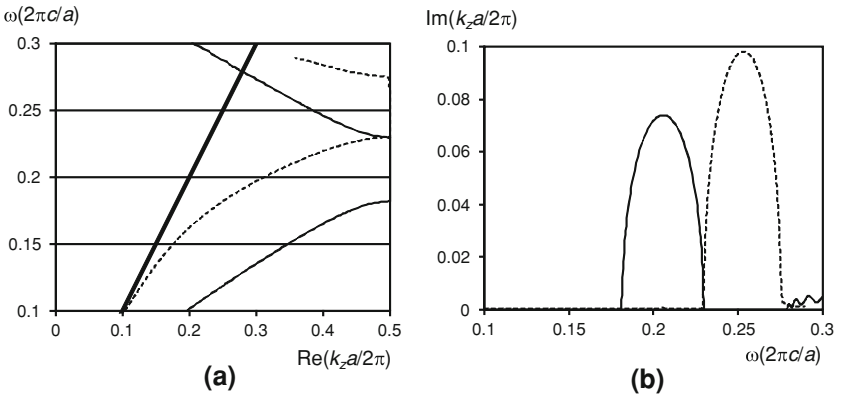

Fig. 3 (**a**) Real and (**b**) imaginary part of the Bloch mode propagation constant k_z versus frequency. Thin (dashed) line presents the FF (SH). The light line is indicated by the thick line in graph (**a**)

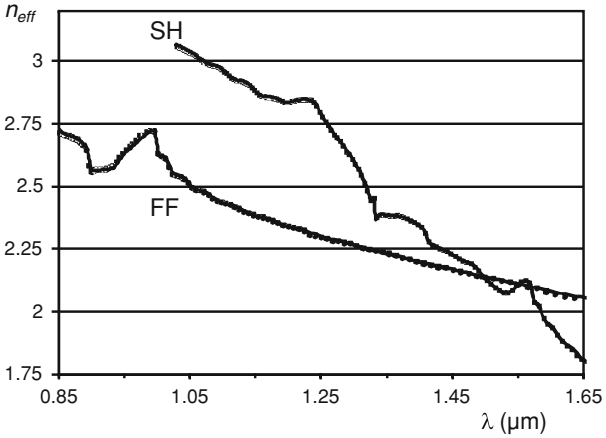

Fig. 4 Effective index at FF and SH versus wavelength λ for a finite device with $N = 20$. The wavelength for the SH is doubled. Dots (lines) present the TD-BPM (EEM) results, respectively

The imaginary part of k_z measures the radiation loss of the Bloch mode. From Fig. 3b we see that the losses around the SHG point are negligible for both frequencies, as both modes lie below the lightline. In a previous design the SH mode was located above the lightline, which rendered the losses too high for efficient conversion. Theoretically the losses of a guided Bloch mode below the lightline are zero. Numerically we indeed obtain negligible values well below 10^{-4}, because of the PML absorbing boundary conditions. At the center of the bandgap the decay is maximal. Note also the losses for the FF above $\omega = 0.28(2\pi c/a)$, as we cross the lightline.

In *finite* structures the concept of phase-matching has been made very precise (Centini et al. 1999). The theory was developed for 1D structures, but it is also applicable in a 2D or 3D context. The effective index n_{eff} is defined from the transmission amplitude t:

$$t(\omega) = \sqrt{|t(\omega)|^2}\exp(jn_{eff}(\omega)Na), \tag{12}$$

with Na the length of the structure. The arbitrariness in n_{eff} is fixed by defining it to be a continuous, increasing function of frequency, and $n_{eff} \to 0$ for $\omega \to 0$. This effective index for both frequencies in a structure with $N = 20$ is plotted in Fig. 4, employing both TD-BPM and EEM. Around the frequencies of interest we notice that $n_{eff}^{FF} \approx n_{eff}^{SH}$. This indicates exact phase-matching and can lead to efficient conversion (Centini et al. 1999).

Another important property is the transmission and reflection of the finite structure. If both frequencies are tuned at a transmission maximum, one expects good SHG. Transmission and reflection magnitudes for the FF are shown in Fig. 5a and b, for $N = 5$ and $N = 20$, respectively. Similar results for the SH are plotted in Fig. 5c and d. Again, both modeling methods are employed and they show a good agreement.

We note that with EEM these spectra are obtained by sweeping over each required frequency. In the TD-BPM each spectrum in Fig. 5 is obtained from a single time-domain run, with a specified center carrier frequency that corresponds to a center wavelength λ_0 of 1.55 μm for the FF pump and $\lambda_0 = 0.775$ μm for the SH wave. The results from the TD-BPM achieve high agreement with the EEM technique around these center wavelengths. Indeed, there the TD-BPM algorithm is expected to achieve its highest accuracy (say over a wavelength range from 1.42 μm to 1.75 μm for the FF field, and from 0.72 μm to 0.82 μm for the

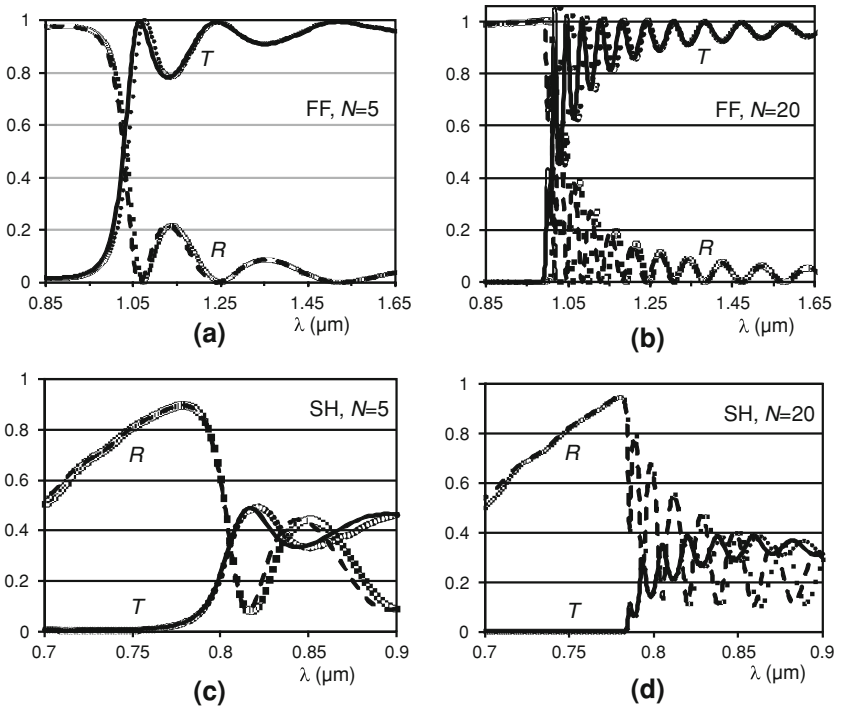

Fig. 5 Transmission T and reflection R versus wavelength λ for the FF ((**a**) $N = 5$, (**b**) $N = 20$) and for the SH ((**c**) $N = 5$, (**d**) $N = 20$). Dots (lines) present the TD-BPM (EEM) results, respectively. TD-BPM uses carrier 1.55 μm for FF and 0.775 μm for SH

SH field). But it is expected to deviate from those of the EEM method at wavelengths further away from the chosen center wavelengths. Thus, for accurate broadband calculations using TD-BPM a number of spectral responses can be stitched together.

We see that the FF transmission spectra show resonances with transmissions close to one. The SH spectra indicate lower transmissions, which are still acceptable. These losses stem from the mismatch at the input and output, between the waveguide mode and the Bloch mode. Reasons for the increased loss at the SH are the higher frequency, different polarization and stronger index contrast.

Note that there is also a connection between n_{eff} of Fig. 4 and the transmission maxima in Fig. 5. More precisely, the maxima of the derivative $\mathrm{d}n_{eff}/\mathrm{d}\omega$ (which is proportional to the density of modes (Dumeige et al. 2002)) correspond to the transmission resonances.

4.2 Nonlinear properties

After having established that the linear properties are designed for efficient conversion, we can examine the full nonlinear simulations. In Fig. 6a and b we show the SHG conversion efficiency spectrum for $N = 5$ and $N = 20$, respectively. The efficiency η is defined as the ratio between the SH power in the output waveguide and the FF power launched into the input waveguide. Remember that we use $\chi^{(2)} = 1$. We notice a very good agreement between both calculation methods.

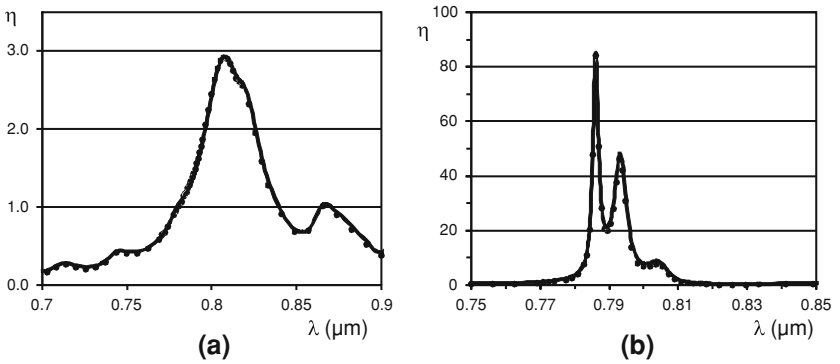

Fig. 6 SHG conversion efficiency η versus SH wavelength λ with: (**a**) $N = 5$ and (**b**) $N = 20$. Dots (lines) present the TD-BPM (EEM) results, respectively

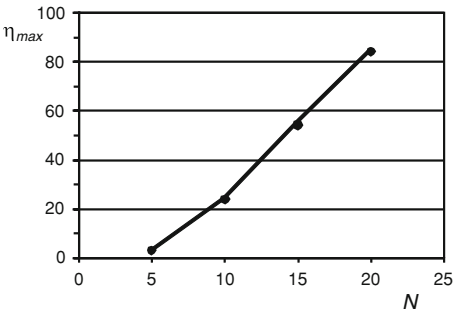

Fig. 7 Maximum SHG conversion efficiency η_{max} versus the number of periods N. The line connects the EEM results, dots show TD-BPM calculations

To get a feel for the maximum conversion efficiency in function of the number of periods N, we provide results for various N in Fig. 7. Results were calculated for $N = 5, 10, 15$ and 20. A higher SHG efficiency can be achieved by increasing the length of the nonlinear structure. The calculations show that the SH conversion efficiency for a 20 period waveguide grating is 30 times larger than the efficiency associated with a 5 period waveguide grating. This is good considering the structure is still very compact, with 20 periods corresponding to a grating length of around 4 μm.

Although difficult to fit with the limited number of points, further analysis shows that the efficiency scales as $N^{2.5}$. This is better than the normal bulk trend of N^2, but still far from the 1D theoretical limit of N^6. One reason is the limited transmission of the resonances at the SH, see Fig. 5c and d, because of losses. A strategy to remedy this is to decrease the diffraction losses by using a broader core, as was done in Dumeige et al. (2003).

5 Conclusions

We present a comparison of linear and nonlinear calculations on a microphotonic device for SHG. The TD-BPM and EEM tools show good agreement and are well suited to tackle these problems.

The proposed device consists of a 2D waveguide with a high-index-contrast 1D grating. We show that the structure is designed to achieve good conversion by adhering to different principles. From a 1D viewpoint efficiency increases because of band-edge and phase-matching

effects. From a 2D viewpoint it is imperative to increase the transmission by limiting the radiation losses.

Acknowledgements BM and PB acknowledge the Flemish Fund for Scientific Research (FWO-Vlaanderen) for postdoctoral fellowships. Parts of this work were performed in the context of the European COST-P11 action and the Belgian DWTC project IAP-Photon. We thank L.C. Andreani, D. Gerace, M. Liscidini and M. Patrini for proposing the COST-P11 SHG modeling exercise.

References

Angelis, C.D., Gringoli, F., Midrio, M., Modotto, D., Aitchison, J., Nalesso, G.: Conversion efficiency for second-harmonic generation in photonic crystals. J. Opt. Soc. Am. B **18**, 348–351 (2001)

Benson, T., Hu, B.B., Vukovic, A., Sewell, P.: What is the future for beam propagation methods?. Proc. Soc. Photo. Opt. Instrum. Eng. **5579**, 351–358 (2004)

Bienstman, P., Baets, R.: Optical modelling of photonic crystals and VCSELs using eigenmode expansion and perfectly matched layers. Opt. Quant. Electron. **33**, 327–341 (2001). CAMFR simulation software is freely available from http://camfr.sourceforge.net/

Bortz, M.L., Fejer, M.M.: Annealed proton-exchanged $LiNbO_3$ waveguides. Opt. Lett. **6**, 1844–1846 (1991)

Centini, M., Sibilia, C., Scalora, M., D'Aguanno, G., Bertolotti, M., Bloemer, M., Bowden, C., Nefedov, I.: Dispersive Properties of finite, one-dimensional photonic band gap structures: applications to nonlinear quadratic interactions. Phys. Rev. E **60**, 4891–4898 (1999)

Chou, H.-F., Lin, C.-F., Wang, G.-C.: Comparisons of Finite Difference Beam Propagation Methods for Modeling Second-Order Nonlinear Effects. J. Lightwave Technol. **17**, 1481–1486 (1999)

Dumeige, Y., Sagnes, I., Monnier, P., Vidakovic, P., Abram, I., Meriadec, C., Levenson, A.: phase-matched frequency doubling at photonic band edges: efficiency scaling as the fifth power of the length. Phys. Rev. Lett. **89**, 043901 (2002)

Dumeige, Y., Raineri, F., Levenson, A., Letartre, X.: Second-harmonic generation in one-dimensional photonic edge waveguides. Phys. Rev. E **68**, 066617 (2003)

Hu, B.: Advanced Beam Propogation Methods for the Analysis of Integrated Photonic Devices. University of Nottingham, PhD thesis (2006)

Hu, B., Sewell, P., Vukovic, A., Paul, J., Benson, T.: General approach for Nth order dispersive material. IEE Proc.-Optoelectron. **153**, 13–20 (2006)

Huang, W., Wu, C., Chu, S.T., Chaundhuri, S.K.: The finite-difference vector beam propagation method: analysis and assessment. IEEE J. Quant. Electron **10**, 295–305 (1992)

Maes, B., Bienstman, P., Baets, R.: Modeling second-harmonic generation by use of mode expansion. J. Opt. Soc. Am. B **22**, 1378–1383 (2005)

Marcuse, D.: Theory of Dielectric Optical Waveguides. Academic Press, New York, NY (1991)

Masoudi, H.M.: A time domain beam-propagation method for analysing pulsed optical beams in second-order nonlinear waveguides. Microwave Opt. Technol. Lett. **28**, 253–257 (2001)

Taflove, A.: Advances in Computational Electrodynamics: the Finite-Difference Time-Domain Method. Artech House, Boston, MA (1998)

Yoo, S.J.B., Caneau, C., Bhat, R., Koza, M.A., Rajhel, A., Antoniades, N.: Wavelength conversion by difference frequency generation in AlGaAs waveguides with periodic domain inversion achieved by wafer bonding. Appl. Phys. Lett. **68**, 2609–2611 (1996)